RSC Advances




ROYAL SOCIETY OF CHEMISTRY

www.rsc.org/advances

# In situ electrosynthesis of hydrogen peroxide with an improved gas diffusion cathode rolling by carbon black and PTFE

Haijian Luo [a], Chaolin Li [a,*], Chiqing Wu [a], Xiaoqing Dong [b]

a. Environmental Science and Engineering Research Center, Shenzhen Graduate School, Harbin Institute of Technology, Shenzhen 518055, PR China.

b Department of Environmental Engineering Technology, Shenzhen Institute of Information Technology, Shenzhen 518172, PR. China

Corresponding author: Chaolin Li

Tel./fax: +86 755 26032455

E-mail address: lichaolin@hitsz.edu.cn

**Abstract:** A simple structure of gas diffusion electrode (GDE) was constructed by rolling carbon black and PTFE as conductive catalyst layer to enhance the producibility of hydrogen peroxide. Box - Behnken design (BBD) coupled with response surface methodology was employed to assess individual and interactive effects of the three main independent parameters (pH, current density, air flow rate) on $H_2O_2$ concentration. Analysis of variance (ANOVA) showed a high coefficient of determination value. Optimal operating conditions were pH value of 4.0, current density of 52 $mA/cm^2$, air flow rate of 55 mL/min. The predicted $H_2O_2$ concentration under the optimum conditions determined by the proposed model was 309.85 mM. It demonstrated that the improved GDE with inexpensive, highly producible and high performance could be produced by rolling method without using noble metal and other chemical promoters. Results also revealed that current density, air flow rate, and their interaction effect had a significant effect on $H_2O_2$ concentration, whereas changes the initial pH left it insensitive. Experiments showed that current density has a direct effect on the decomposition reaction in the electrolytic process.

**Keywords:** Hydrogen peroxide; Electrosynthesis; Gas diffusion cathode; Carbon black; Decomposition

## 1. Introduction

Hydrogen peroxide ($H_2O_2$), as a versatile oxidizing agent, has been widely used in many industrial areas, particularly in the chemical industry and environmental domain. The only degradation product of its use is water, thus it has played an important role in environmentally friendly methods in the chemical industry [1, 2]. So far, $H_2O_2$ is produced on an industrial scale by the anthraquinone oxidation (AO) process. However, it can hardly be considered a green method, since the processes involves the sequential hydrogenation and oxidation of an alkylanthraquinone precursor dissolved in a mixture of organic solvents followed by liquid–liquid extraction to recover $H_2O_2$ [1]. The transport, storage, and handling of bulk $H_2O_2$ involve hazards and escalating expenses [3]. Thus, novel, cleaner methods for the in-situ production of $H_2O_2$ are being explored.

Various procedures are available for in situ synthesis of $H_2O_2$, including direct synthesis of $H_2O_2$ from $O_2$ and $H_2$ catalyzed by a variety of catalyst [4] or activated by dielectric barrier discharge[5], application of microbial fuel cells [6]. However, these methods are characterized by several limitations, such as the necessity to remove the employed catalyst, high cost of catalytic materials. On the contrary, electrosynthesis methods present various advantages, e.g., the use of catalysts immobilized in the electrode structure, and the inexpensive carbonaceous materials with the high catalytic performance for $H_2O_2$ production [7]. Carbon materials is an excellent cathode for two-electron reduction of oxygen to $H_2O_2$ and is the prime choice for an electrocatalyst support because of its large specific surface area, good thermal and chemical stability, and low price [8] .

Of all the electrode structure, gas diffusion electrode (GDE) has attracted great attention owing to its relatively high $H_2O_2$ production [9-12]. The GDE is composed of an active layer and a gas diffusion layer, which allows an unlimited supply of gaseous reagents to pass through the porous structure to the electrode/electrolyte interface, thus preventing mass transport limitation of the

reaction of interest [7, 13] . In the electrolytic process, the catalytic layer faces to electrolyte while the gas diffusion layer faces the reactant gas that diffuses through micro-pores of the GDE to the catalytic layer and reacts with electrolyte at the interface between the electrolyte and the reactant gas[9, 14]. Depending different cathode materials and electrode construers, the $H_2O_2$ yield and current efficiency differed much. But most of these cathodes in the $H_2O_2$ yield and current efficiency are insufficient for its application of in situ electrosynthesis. Therefore, novel cathode, with high efficiencies and low costs, must be developed. So far, GDE using as cathode for in situ electrosynthesis of $H_2O_2$ have been mainly focused on various carbon-based materials (e.g., graphite, carbon nanotube, carbon black) [13, 15-17] and its modification (e.g., modified by 2-ethylanthraquinone, azobenzene) [13, 18], and its application for degradation of different organic pollutants [16, 19-22]. However, the effects of the cathodes construction were usually neglected, which is absolutely vital for process effectiveness [23]. In the present work, an improved GDE prepared by rolling carbon black and polytetrafluoroethylene was introduced to the electrolytic process. Compared with the conventionally used GDE system, the improved GDE was proved greatly enhancing $H_2O_2$ productivity and accumulation.

Except for cathode properties, the operating conditions have significant impacts on $H_2O_2$ productivity and current efficiency . It is well documented in the literature that how the efficiency of the electrolytic process depends on the pH, current density, air flow rate, supporting electrolyte and electrolytic time [2, 7, 24, 25]. With typical multifactor experiments, different operating conditions should therefore be employed to achieve higher $H_2O_2$ concentration and its current efficiency. While in typical multifactor experiments, optimal conditions of these variables are usually carried out by varying a single factor while keeping the other variables constant, the methodology does not include possible interaction effects between variables and could lead to restricted conclusions [26, 27].

The response surface methodology (RSM) is a widely accepted statistical-based method for designing experiments, evaluating the individual and interaction effects of independent variables, and optimizing the process parameters with limited number of experiments [28]. For example, according to the oxygen reduction reaction ($O_2 + 2H^+ + 2e^- \rightarrow H_2O_2$), is influenced by applied current, pH value and gas flow rate simultaneously. Operating process optimization by RSM is faster for collecting experiment results than the rather conventional, time consuming one-factor-at-a-time approach [29].

In this work, an improved GDE was proposed to enhance the electrochemical performance during the electrolytic process. The RSM based on Box - Behnken design (BBD) was employed to design and optimize individual and interactive effects of the four main independent parameters (initial pH, current density and air flow rate) on $H_2O_2$ accumulation. The significance of each variable on the $H_2O_2$ concentration was determined and the optimal operating condition was obtained and validated.

## 2. Experimental section

### 2.1 Materials

The carbon black powder (CB), Vulcan XC 72R, was purchased from Cabot Corporation and used without any treatment. The particle size distribution and the nitrogen adsorption isotherm of the samples are show in Fig. S1. Polytetrafluoroethylene (PTFE, 60 wt%, Hesen, Shanghai, China) was used as binder. Nafion-117 (Dupont, New York, NY, USA) was used as the cation-exchange membrane.

### 2.2 Preparation procedure of gas diffusion cathode

The improved gas diffusion cathode (IGDE) consisted of a conductive catalytic layer (CCL) and a titanium meshes. Different from traditional GDE comprise by gas diffusion layer and catalyst

layer [22, 30], the CCL simultaneously acts both as gas diffusion layer and catalyst layer. After a hydrophobic treatment with PTFE, the titanium mesh (40 meshes) was used as the matrix.

The IGDE fabrication procedures are presented in Fig. 1. The CCL was prepared firstly by distributing CB powder of 2.0 g into an appropriate amount of dispersant (ethanol) in a beaker and ultrasonic agitated for 20 min at room temperature, followed by dripping 60 wt % PTFE suspensions of 0.83 g (CB: PTFE = 4: 1) into the blend slowly. After stirred uniformly, the mix was still operated with ultrasonic agitation to disperse the carbon black and PTFE particles to form fine networks of gas channels [23]. The blend was stirred and the redundant alcohol was removed to give a paste. The paste was just rolled on the either side of the hydrophobic titanium mesh to be a flat sheet of 0.8 mm thickness. The flat sheet was thermolaminated by mean of thermal compression bonding method to obtain the final IGDE of 0.5 mm thickness. The pressure and the temperature of the hot-pressing process was 10 MPa and 100 ºC, respectively. Then the sheet was then sintered for 10 min at 300 ºC to sinter the PTFE in order to form the fibrous three-dimensional structure for gas transport [31].

### 2.3 Electrolytic procedures

The electrolytic process were performed in an divided three-electrode cell under constant current mode with a potentiostat (CH Instruments, Chenhua, Shanghai, China). A cation exchange membrane (Nafion-117) was used to separate the two chambers. The three chambers were for cathode gas, catholyte and anolyte. The cathodic and anodic chamber had a volume of 15 mL and 30 mL, respectively. An aqueous solution of 0.2 mol/L $Na_2SO_4$ was used as supporting electrolyte and the initial pH was adjusted by $H_2SO_4$ or NaOH. Air was used as oxygen sources. The prepared IGDE (5 cm×2 cm) used as working electrode, a platinum plate (1 cm ×1 cm ) was used as the anode because of its overpotential and high chemical stability. the distance between electrodes was 1.5 cm. A schematic diagram of the experimental setup was shown in Fig. 2.

Reaction solutions were collected to determine the $H_2O_2$ concentration after electrolysis. The yield of $H_2O_2$ was determined by a chemical titration with an aqueous solution of $KMnO_4/H_2SO_4$. Current efficiency (CE) of $H_2O_2$ formation was calculated from the two-electron reaction against the quantity of charge passed and measured by a coulomb meter (Eq 1).

$$CE = \frac{2F \times H_2O_2 \text{ yield}}{\text{quantity of charge passed}} \times 100\% \qquad (1)$$

Where F is the Faraday constant of 96485 C $mol^{-1}$.

**2.4 . Experimental design and statistical model**

The optimization of experimental conditions for $H_2O_2$ electrosynthesis by IGDE was conducted using Box–Behnken design (BBD) technique under RSM. The software Design Expert 8.0 was used for the experimental design, data analysis, quadratic model buildings, and graph plotting. The independent variables of initial pH, current density and air flow rate were coded with low and high levels in BBD as shown in Table 1, while the response was expressed $H_2O_2$ concentration after 1 h reaction. The results along with the experimental conditions are presented in table 2.

The experimental results of the BBD were fitted with a quadratic model as below[26]:

$$Y = k_0 + k_aA + k_bB + k_cC + k_{ab}AB + k_{ac}AC + k_{bc}BC + k_{aa}A^2 + k_{bb}B^2 + k_{cc}C^2 \qquad (2)$$

where Y is the predicted response; $k_0$ is a constant; $k_a$ , $k_b$ , $k_c$ are the linear coefficients; $k_{ab}$, $k_{ac}$, $k_{bc}$ are the cross-coefficients; $k_{aa}$, $k_{bb}$, $k_{cc}$ are the quadratic coefficients.

The Pareto analysis ($P_i$) [32] gives more significant information to interpret the results. In fact, this analysis calculate the percentage effect of each factor on the response, according to the following relation:

$$P_i = \left(\frac{b_i^2}{\sum b_i^2}\right) \times 100 \quad (i \neq 0) \qquad (3)$$

Variances analysis (ANOVA) was conducted to analyze the results and to verify the statistical

significance of the fitted quadratic models. The interaction between the process variables was illustrated by the three-dimensional (3D) response surface and two-dimensional (2D) contour plots. The optimum process parameters for the electrolytic process were calculated using the fitted models and validated by the experiments.

## 3. Results and discussion

### 3.1 In situ electrosythesis of $H_2O_2$ by IGDE

The performance of IGDE for $H_2O_2$ electrosythesis was tested under the conditions of various current density at pH 3.0, air flow rate 40 mL/min, 0.2 mol/L $Na_2SO_4$. An apparent increase in $H_2O_2$ concentration and a gradually decrease in current efficiency with electrolytic time are present in Fig. 3 (a) and (b). The IGDE at the current density of 60 mA/cm$^2$ exhibits a higher catalytic activity toward oxygen reduction generating $H_2O_2$ than that at 40 and 80 mA/cm$^2$. In this case, a maximal $H_2O_2$ accumulation of 315.67 mM was achieved by electrolysis of 120 min, and then there is no obvious improvement of $H_2O_2$ concentration. This behavior can be explained assuming that, in the steady state, $H_2O_2$ is electrogenerated and simultaneously destroyed at the same rate in the electrolytic process. These results confirm that the novel preparation procedure of IGDE was an effective way for improving the $H_2O_2$ concentration. Table 3 describes an extensive summary of $H_2O_2$ accumulation using different electrode structure found in literature. Comparably, a higher $H_2O_2$ concentration was obtained compared with other GDE reported in publication, indicating that the IGDE an efficient cathode for $H_2O_2$ accumulation.

It is known that the electrode structure greatly influences the performance of $H_2O_2$ generation, especially its accumulation [9]. Indeed, all of carbon material catalysts so far identified for $H_2O_2$ electrosynthesis are equally effective for its sequential hydrogenation or decomposition to water [33]. As a result, higher current efficiency would be achieved at early stage and gradually decrease with

the increasing $H_2O_2$ concentration. We have now addressed this problem and show that the IGDE can reduce the sequential hydrogenation and decomposition of $H_2O_2$, there by producing high $H_2O_2$ accumulation. Additionally, the $H_2O_2$ production rate in earlier periods is higher than in later ones, inferring that $H_2O_2$ is also chemically descomposed to $H_2O$ at the IGDE surface.

The surface morphologies of the CCL exposing to the electrolyte were scanned at a magnification of 10,000. The SEM images were presented from Fig. 4. The ropiness networks should be formed by rolled PTFE which bound CB particles together and form the air transport channels. From these images, it was clearly showed that the cross-linked networks gradually increased with the decrease of CB/PTFE ratio. It has been proved that oxygen reduction reaction (ORR) takes place at the three-phase interface catalyst–air–electrolyte [34]. The solid phase provides electron transport and catalyzes the ORR, and the gas phase is responsible for gas diffusion, whereas the liquid phase ensures the proton supply and the production diffusion [31]. PTFE is a usual binding material used in the preparation of gas diffusion oxygen reducing electrodes for its hydrophobic properties facilitating the oxygen permeability and diffusion. Moreover, PTFE also provides hydrophobicity and enhances the air permeability [2]. Insufficient PTFE content brings about the uneven distribution of the pore channel, even the large cross-section connection (Fig. 4 a). The airflow could pass easily through form the large channel, while the other compacted surface hardly contact with air, which cause insufficient or absent oxygen to the two-electron reaction. There were still numbers of macro pores and cross-linked ropiness existed uniformly throughout the CCL even though the CB/PTFE ratio reached to 1. However, excessive amounts of PTFE evolve into the formation of the PTFE film, which covering on the CCL surface Fig.4 c. For this reason, the active sites of GDE for catalyzing the reduction of oxygen gas to $H_2O_2$ were reduced sharply. Consequently, the maximum $H_2O_2$ concentration was obtained at CB/PTFE ratio of 4 because of its uniform channel and adequate active site (Fig. 4 b.).

### 3.2. Fitting model and analysis of variance

According to the experimental results, an empirical relationship between the response and independent variables was attained and expressed by the following second-order polynomial equation:

$$Y = 313.40 - 5.65A + 26.85B + 18.69C - 8.16AB + 5.70AC + 15.12BC - 51.14A^2 - 146.27B^2 - 53.71C^2 \quad (3)$$

The data of $H_2O_2$ concentration was fitted to the quadratic models, and the significance and the adequacy were tested by the ANOVA. The ANOVA results present in Table 4. P-value less that 0.050 indicates that the model terms are significant at 95 % confidence level or more, while the values greater than 0.100 are usually considered as insignificant [35]. The model predicted by Eq. 3, P value less 0.0001 shows that these are significant for describing the $H_2O_2$ concentration.

These results (Table 5) show that the regression model had a high value of coefficient of determination ( $R^2$ = 0.999).The $R^2$ -value provides a measure of how much variability in the observed response values can be explained by the experimental factors and their interactions. This implies that 99.9% of the variations for $H_2O_2$ concentration are explained by the independent variables and this also means that the model does not explain 0.1% of variation. The value of the adjusted determination coefficient (adjusted $R^2$ = 0.9968) also proved the high significance of the model. Additionally, the low value of the coefficient of variation (C.V. = 2.56%) suggested the high precision and reliability of the experiment. In addition, the F -test of the regression models produced very low p-values (<0.0001), indicating that the model was of high significance. According to the above explained ANOVA test results, the model application explained the reaction quite well and can be employed to navigate the design space at least in terms of $H_2O_2$ concentration.

Fig. 5 represents the Pareto graphic analysis. It shows that current density, air flow rate and

initial pH are the most determining factors on $H_2O_2$ concentration, their effect is over 90% on the investigated response.

As shown in Fig. 6, the comparison of actual and predicted $H_2O_2$ concentration of the process efficiency shows that the predicted data are in good agreement with the experimental ones. Therefore, the regression models can be used to predict the $H_2O_2$ concentration from the initial experimental conditions.

### 3.3. Response surface and contour plots

Factors giving significant interaction effects in the new simplified fitted models were chosen for the axes of the response surface plots to account for curvature of the surfaces [36]. The object of this work aims at enhancing $H_2O_2$ concentration rather than CE, thus the following research just focus on the $H_2O_2$ concentration. The three-dimensional (3D) response surface and two-dimensional (2D) contour plots of the model-predicted responses, while other variables kept at constant and the others varying within the experimental ranges were utilized to assess the interactive relationships between the process variables and $H_2O_2$ concentration.

#### 3.3.1 Effect of initial pH and current density

The effect of initial pH and current density on $H_2O_2$ concentration is illustrated in Fig. 7. The peak shown in the contour plot indicates that the highest $H_2O_2$ concentration is achieved in the range located in that circular contour. It illustrate that there is an obvious interaction between initial pH and current density on $H_2O_2$ concentration. $H_2O_2$ concentration increased sharply with increasing current density at all kinds of initial pH until the current density above 55 mA/cm$^2$, and then it decrease with the current density increasing. The results also show that the highest $H_2O_2$ concentration was obtained in the pH 4.0, and it was affected by too high or too low pH value.

In this study, a cation exchange membrane (Nafion-117) was used to separate the two

electrolytic cells. It obstructs the penetration of anions and $H_2O_2$ molecules, but allows cations ( $H^+$ and $Na^+$), to freely penetrate through it [2]. Therefore, $H_2O_2$ at the cathode will be confined in the cathode chamber, avoiding its decomposition at the anode. In the electrolytic process, protons electrolyzed at the anode chamber will be electrically driven to the cathode chamber, partially supplementing the protons consumption.

Fig. S2 shows the pH values as the function of electrolytic time. In the diaphragm electrolytic device, it could keep the pH < 1 (Eq. 8) in anode chamber after 10 min electrolysis because the oxidation of $H_2O$ releases oxygen gas and protons at the anode (Eq.5). In case of the cathode chamber, initial pH below 2 keep the electrolyte acidic in the whole electrolytic process, while the pH rapidly becomes to alkaline when the initial pH above 4. It has been reported that $H_2O_2$ can be electrochemically generated by oxygen reduction reaction (ORR) in both acidic (Eq.6) [2] and alkali solutions (Eq.7) [37]. Therefore, high $H_2O_2$ concentration was obtained whether the original solution was acidic, neutral or alkaline solution.

$$2H_2O \rightarrow 4H^+ + O_2 + 4e^- \qquad (5)$$

$$\text{Alkaline medium: } H_2O + O_2 + 2e^- \rightarrow HO_2^- + OH^- \qquad (6)$$

$$\text{Acidic medium: } O_2 + 2H^+ + 2e^- \rightarrow H_2O_2 \qquad (7)$$

**3.3.2 Effect of air flow rate and current density**

Fig. 8 shows the response surface assuming current density and air flow rate as independent factors. The peak shown in the contour plot indicates that the highest $H_2O_2$ concentration is achieved in the range located in that circular contour. There is an optimum value of the current density for each air flow rate level. It is evident that there is an obvious interaction between the current density and air flow rate on $H_2O_2$ concentration. As shown in Fig. 3, current density play an important role in $H_2O_2$ concentration. The $H_2O_2$ concentration dropped dramatically once the

current density above 60 mA/cm$^2$, leading to a low CE.

These results can be explained by using the cell potential. During electrolytic process, $H_2O_2$ is produced at the cathode surface through ORR in the acidic or alkaline medium. However, side reactions simultaneously occur in the electrolytic process [2]: (a) four-electron reaction (Eq. 8), (b) decomposition reaction (Eq. 9 and 10) due to the $H_2O_2$ accumulation at the GDE interface, and (c) hydrogen evolution reaction (Eq.11).

$$O_2 + 4H^+ + 4e^- \rightarrow 2H_2O \qquad (8)$$

$$\text{Acidic medium: } H_2O_2 + 2H^+ + 2e^- \rightarrow 2H_2O \qquad (9)$$

$$\text{Acidic medium: } H_2O_2 + HO_2^- \rightarrow H_2O + O_2 + OH^- \qquad (10)$$

$$2H^+ + 2e \rightarrow H_2 \qquad (11)$$

To confirm the effects of the side reactions on $H_2O_2$ concentration, a electrolyte containing 1.0 wt % $H_2O_2$ was add into cathode chamber. The reaction parameters represent the optimum conditions established for the synthesis of $H_2O_2$. The only difference was that pure nitrogen, instead of air, as the gas source. The results are shown in Fig. 9. The amount of $H_2O_2$ decomposition increasing with the increasing electrolytic time. Moreover, this phenomenon is more remarkable when the current density higher than 60 mA/cm$^2$. The inset panel of Fig. 9 shows the variation of cell potential with current density. It indicates that the voltage higher than 5.0 V (40 mA/cm$^2$) accelerate the $H_2O_2$ decomposition reaction, demonstrating the decomposition reaction in the electrolytic process was the major reason to inhibit the $H_2O_2$ accumulation. Besides, the ORR through Eq. (7) leads to the formation of $H_2O$ instead of $H_2O_2$ through Eq. (2) at potential values higher than 4.3 V [24, 38]. Indeed, a high potential values should be supplied to the system to get the high current density, which accelerates the decomposition of $H_2O_2$. Moreover, the competitive electrode reactions such as the discharge of hydrogen evolution reaction inhabit the generation of

$H_2O_2$ [7].

### 3.3.3 Effect of initial pH and air flow rate

Fig. 10 illustrates the response surface assuming air flow rate and pH as independent factors. As aforementioned, high $H_2O_2$ concentration were obtained under all working conditions. For a constant initial pH, $H_2O_2$ concentration in the cathode chamber was roughly proportional to applied current in an air flow rate, and a steady-state condition is rapidly reached. But there was considerable decrease in the amount of $H_2O_2$ concentration when the air flow rate was fixed at the high level (over 50 mL/min).

The increase of $H_2O_2$ concentration with increasing gas flow rate can be explained by two major perspectives suggest themselves. First, the origin of the effect could be due to oxygen is consumed in the $H_2O_2$ electrosynthesis by two-electron reaction (Eq.6 or 7) and in the nonselective production of $H_2O$ by four-electron reaction (Eq.8). Second, the hydrodynamics determine the rate of mass transfer between the liquid phase and the GDE surface [39]. A $H_2O_2$ concentration gradient over the GDE surface is created, increasing the $H_2O_2$ decomposition reaction rate. It is physically analogous to increasing the stirring rate in a batch reactor. Thus, enhancing air flow rate promote the mass transfer rate, which is beneficial to the $H_2O_2$ accumulation.

As the air flow rate increased, the $H_2O_2$ concentration increased to the maximum at the gas flow rate of 50 mL/min, after that point no further increase in $H_2O_2$ was observed. It is seen that a rate of 50 mL/min is adequate to maintain the steady-state oxygen during electrolytic process. At higher gas flow rates, the mass transfer between the GDE surface and electrolyte will increase, but probably more important is the increase in the mass transfer through the liquid layer surrounding the catalyst surface, resulting in the low catalytic efficiency [39].

### 3.4. Determination of optimal conditions for electrosynthesis of $H_2O_2$ and verification

In case of multiple responses, RSM describe a range of specific operating conditions that at least keeps them in the desired ranges or in some sense maximizes all responses [35]. In this study, the desired goals in terms of $H_2O_2$ concentration was defined as maximization to achieve highest electrosynthesis performance. $H_2O_2$ concentration contour plots in Fig. 7, 8 and 10 show clear peak areas, demonstrating that the optimum conditions of initial pH, current density and air flow rate were within the design boundary. Accordingly, the optimum values of the process variables were demonstrated in Table 6. After verification through further experiments with the predicted values, it indicates that the maximum $H_2O_2$ accumulation was obtained when the values of each factor were set as the optimum values. The results imply that the strategy to optimize the operating conditions and to obtain the maximum $H_2O_2$ concentration by RSM for the electrolytic process was successful.

## 4. Conclusions

This work has demonstrated that the improved GDE constructed by rolling carbon black and PTFE as conductive catalyst layer was an efficient cathode for $H_2O_2$ accumulation. The main reason hindering $H_2O_2$ accumulation was the subsequent decomposition reaction on the IGDE surface. Response surface methodology (RSM) based on Box-Behnken design (BBD) was employed to assess the individual and interactive effects of several critical process conditions on $H_2O_2$ concentration, and to optimize the electrolytic process. The result of ANOVA shown that the regression model was of high significance and can be used to predict the $H_2O_2$ accumulation form the initial experimental conditions. The optimal conditions for $H_2O_2$ concentration were found to be initial pH 4.0, current density of 52 mA/cm$^2$, air flow rate of 55 mL/min. Under the optimal conditions, the $H_2O_2$ concentration was 309.85 mM after 60 min electrolysis. The obtained results demonstrated the usefulness of response surface methodology in predicting the electrolytic process

as well as the interactive effects of manipulating process variables.

**Acknowledgements**

This work was supported by National Natural Science Foundation of China (Grant No. 51408370). The authors are also greatly appreciated to Wenxiang Zhang (University of Technology of Compiegne, France) for reviewing the manuscript and his suggestive comments.

**References**

1. J. M. Campos‐Martin, G. Blanco‐Brieva and J. L. Fierro, *Angew. Chem. Int. Ed.*, 2006, **45**, 6962-6984.
2. Z. Qiang, J.-H. Chang and C.-P. Huang, *Water Res.*, 2002, **36**, 85-94.
3. T. Murayama and I. Yamanaka, *J. Phys. Chem. C*, 2011, **115**, 5792-5799.
4. M. Teranishi, S.-i. Naya and H. Tada, *J. Amer. Chem. Soc.*, 2010, **132**, 7850-7851.
5. F. Thevenet, J. Couble, M. Brandhorst, J. Dubois, E. Puzenat, C. Guillard and D. Bianchi, *Plasma Chem. Plasma Process.*, 2010, **30**, 489-502.
6. I. Yamanaka, S. Tazawa, T. Murayama, R. Ichihashi and N. Hanaizumi, *ChemSusChem*, 2008, **1**, 988-992.
7. R. M. Reis, A. A. Beati, R. S. Rocha, M. H. Assumpcao, M. C. Santos, R. Bertazzoli and M. R. Lanza, *Ind. Eng. Chem. Res.*, 2011, **51**, 649-654.
8. M. Assumpção, R. De Souza, D. Rascio, J. Silva, M. Calegaro, I. Gaubeur, T. Paixão, P. Hammer, M. Lanza and M. Santos, *Carbon*, 2011, **49**, 2842-2851.
9. X. Yu, M. Zhou, G. Ren and L. Ma, *Chem. Eng. J.*, 2015, **263**, 92-100.
10. R. B. Valim, R. M. Reis, P. S. Castro, A. S. Lima, R. S. Rocha, M. Bertotti and M. R. Lanza, *Carbon*, 2013, **61**,

236-244.

11. M. Giomo, A. Buso, P. Fier, G. Sandonà, B. Boye and G. Farnia, *Electrochim. Acta*, 2008, **54**, 808-815.

12. M. Panizza and G. Cerisola, *Electrochim. Acta*, 2008, **54**, 876-878.

13. J. Forti, J. Nunes, M. Lanza and R. Bertazzoli, *J. Appl. Electrochem.*, 2007, **37**, 527-532.

14. Y. Sheng, S. Song, X. Wang, L. Song, C. Wang, H. Sun and X. Niu, *Electrochim. Acta*, 2011, **56**, 8651-8656.

15. M. Assumpção, R. De Souza, R. Reis, R. Rocha, J. Steter, P. Hammer, I. Gaubeur, M. Calegaro, M. Lanza and M. Santos, *Appl. Catal., B*, 2013, **142**, 479-486.

16. X. Zhang, J. Fu, Y. Zhang and L. Lei, *Sep. Purif. Technol.*, 2008, **64**, 116-123.

17. C. McDonnell-Worth and D. R. MacFarlane, *RSC Adv.*, 2014, **4**, 30551-30557.

18. J. Forti, R. Rocha, M. Lanza and R. Bertazzoli, *J. Electroanal. Chem.*, 2007, **601**, 63-67.

19. G. Xia, Y. Lu and H. Xu, *Electrochim. Acta*, 2015, **158**, 390-396.

20. F. Yu, M. Zhou and X. Yu, *Electrochim. Acta*, 2015, **163**, 182-189.

21. W. Zhang, G. Huang, J. Wei and D. Yan, *Desalination*, 2013, **311**, 31-36.

22. Q. Shi, H. Wang, S. Liu and Z. Bian, *RSC Adv.*, 2014, **4**, 56263-56272.

23. H. Dong, H. Yu, X. Wang, Q. Zhou and J. Feng, *Water Res.*, 2012, **46**, 5777-5787.

24. A. Khataee, M. Safarpour, M. Zarei and S. Aber, *J. Electroanal. Chem.*, 2011, **659**, 63-68.

25. A. Moraes, M. Assumpção, R. Papai, I. Gaubeur, R. Rocha, R. Reis, M. Calegaro, M. Lanza and M. Santos, *J. Electroanal. Chem.*, 2014, **719**, 127-132.

26. T. Xu, Y. Liu, F. Ge, L. Liu and Y. Ouyang, *Appl. Surf. Sci.*, 2013, **280**, 926-932.

27. Z. Zhang and H. Zheng, *J. Hazard. Mater.*, 2009, **172**, 1388-1393.

28. J. Virkutyte, E. Rokhina and V. Jegatheesan, *Bioresour. Technol.*, 2010, **101**, 1440-1446.

29. M. Alim, J.-H. Lee, C. Akoh, M.-S. Choi, M.-S. Jeon, J.-A. Shin and K.-T. Lee, *LWT- Food Sci. Technol.*, 2008, **41**, 764-770.

30. H. Wang and J. Wang, *Electrochim. Acta*, 2008, **53**, 6402-6409.

31. C. Santoro, K. Artyushkova, S. Babanova, P. Atanassov, I. Ieropoulos, M. Grattieri, P. Cristiani, S. Trasatti, B. Li and A. J. Schuler, *Bioresour. Technol.*, 2014, **163**, 54-63.

32. A. R. Khataee, M. Zarei and L. Moradkhannejhad, *Desalination*, 2010, **258**, 112-119.

33. J. K. Edwards, B. Solsona, E. Ntainjua, A. F. Carley, A. A. Herzing, C. J. Kiely and G. J. Hutchings, *Science*, 2009, **323**, 1037-1041.

34. H. Dong, H. Yu, H. Yu, N. Gao and X. Wang, *J. Power Sources*, 2013, **232**, 132-138.

35. I. Arslan-Alaton, G. Tureli and T. Olmez-Hanci, *J. Photochem. Photobiol., A*, 2009, **202**, 142-153.

36. H. Li, S. Zhou, Y. Sun and J. Lv, Waste Manage., 2010, **30**, 2122-2129.

37. V. Antonin, M. Assumpção, J. Silva, L. Parreira, M. Lanza and M. Santos, *Electrochim. Acta*, 2013, **109**, 245-251.

38. A. Özcan, Y. Şahin, A. S. Koparal and M. A. Oturan, *J. Electroanal. Chem.*, 2008, **616**, 71-78.

39. S. J. Freakley, M. Piccinini, J. K. Edwards, E. N. Ntainjua, J. A. Moulijn and G. J. Hutchings, *ACS Catal.*, 2013, **3**, 487-501.

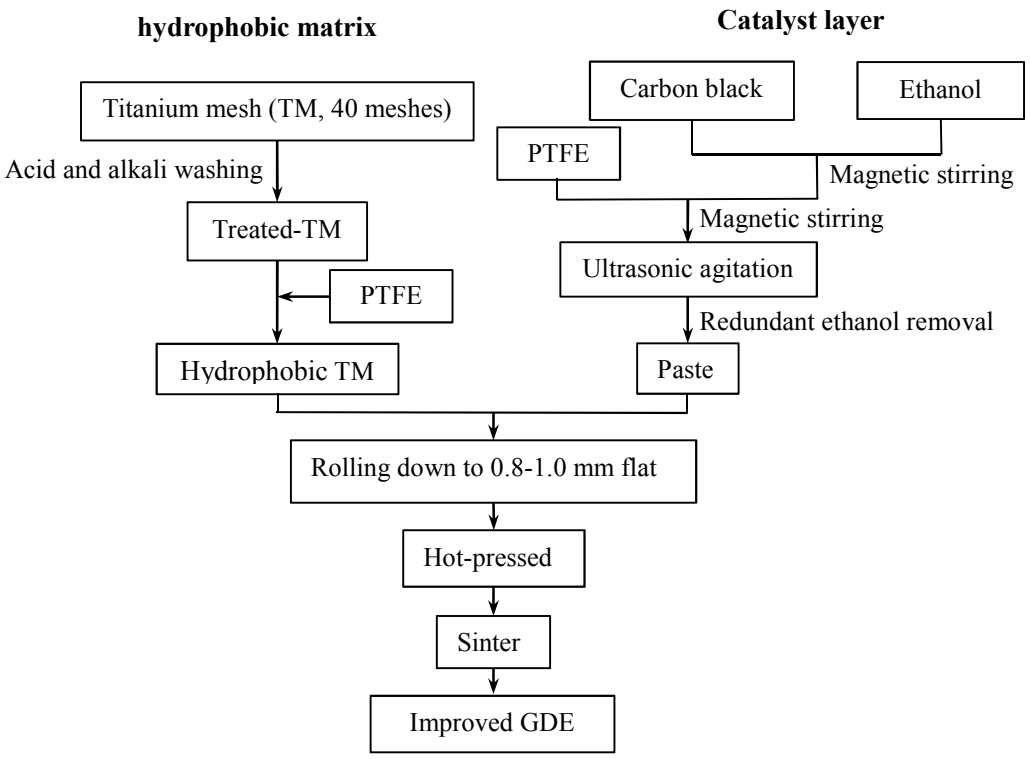


Fig. 1 Fabrication procedures for the novel GDE.

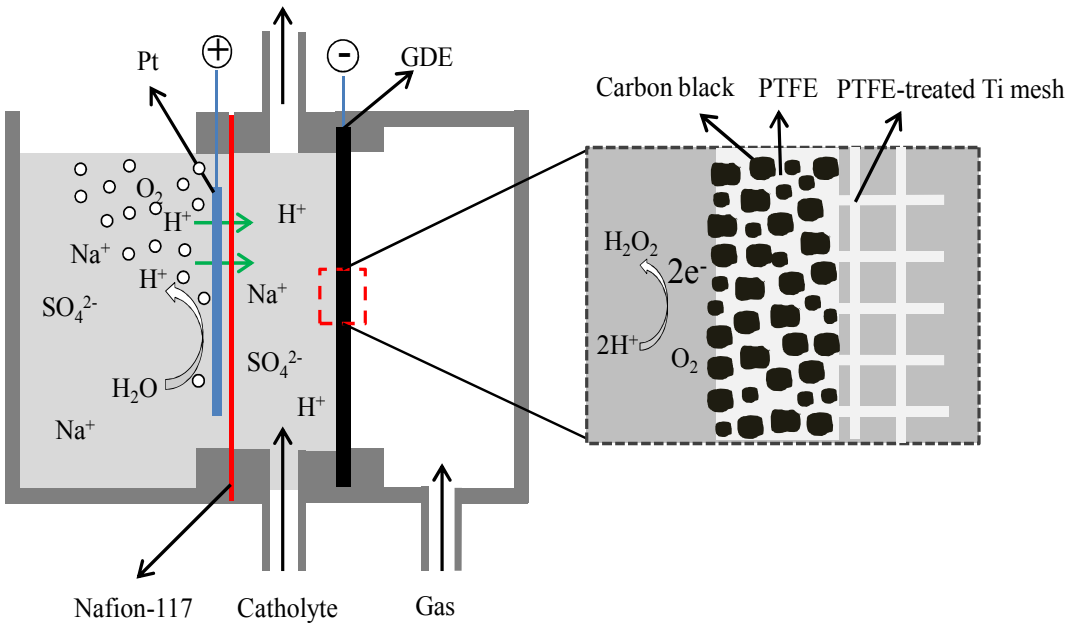


Fig. 2 Schematic diagram of the experimental setup.

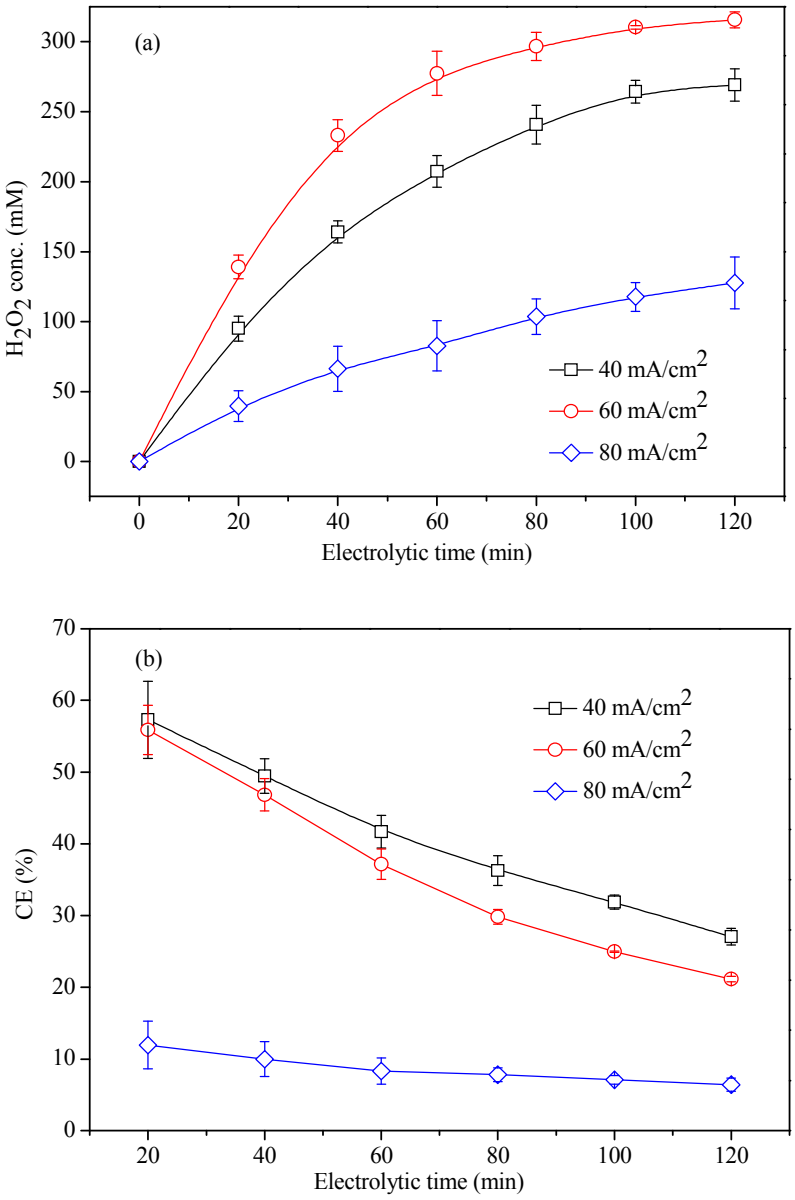


Fig. 3 Effects of current density on (a) $H_2O_2$ concentration and (b) current efficiency. Reaction conditions: pH 3.0, air flow rate 40 mL/min, 0.2 mol/L $Na_2SO_4$.

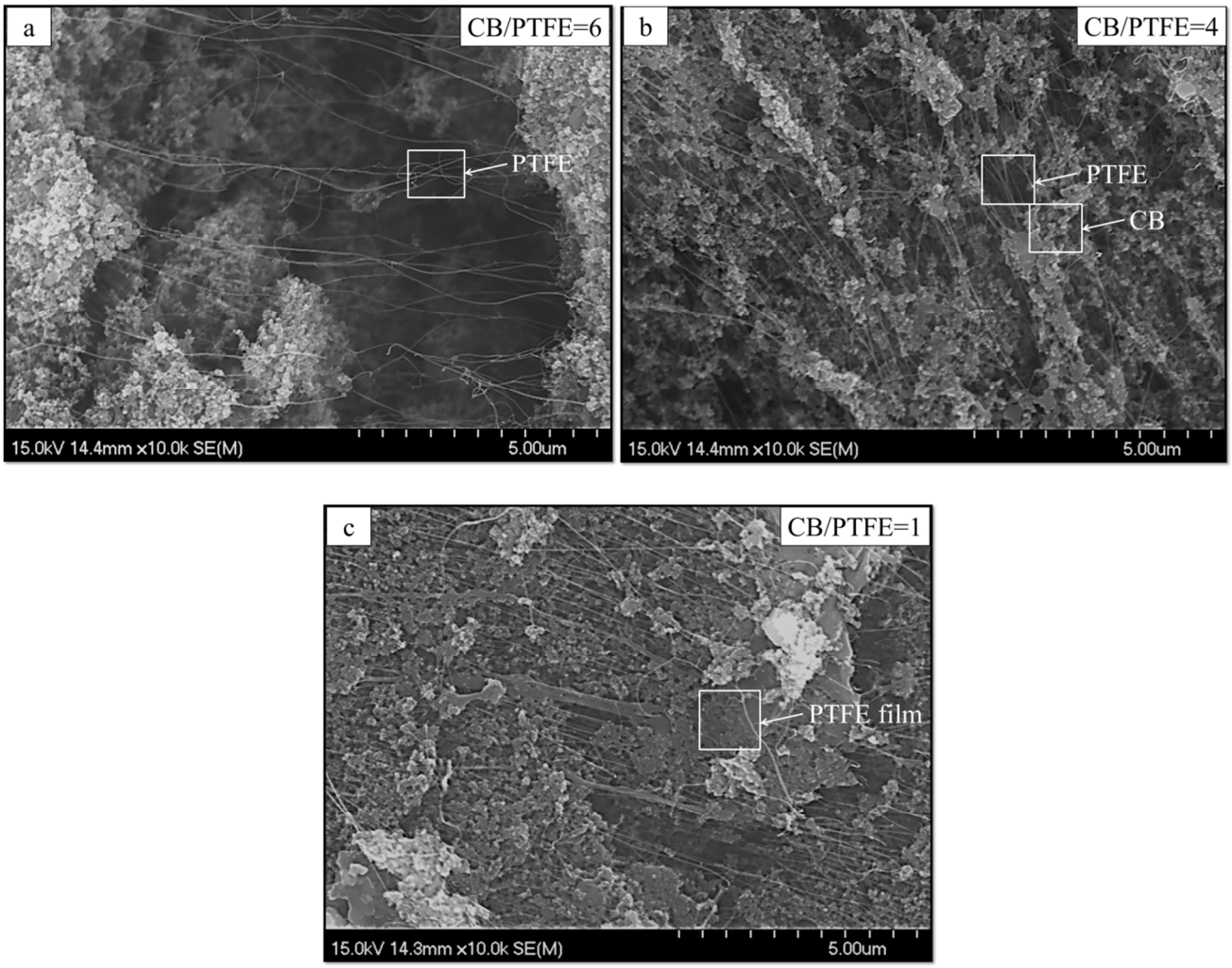


Fig. 4 SEM images of the conductive catalyst layer surface of the IGDEs with (a) CB/PTFE=6, (b) CB/PTFE=4, (c) CB/PTFE=1.

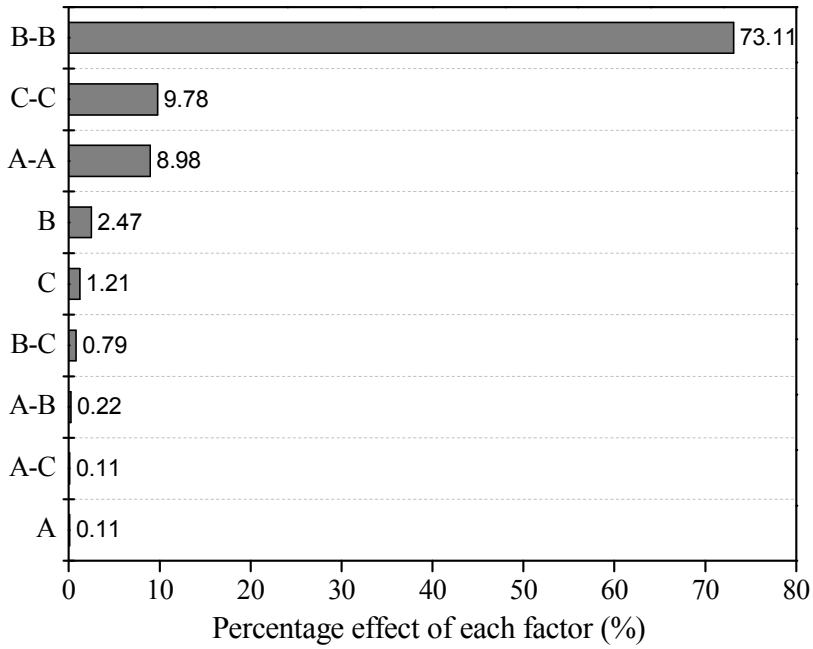


Fig. 5 Pareto graphic analysis. A: initial pH, B: current density (mA/cm$^2$), C: gas flow rate (mL/min).

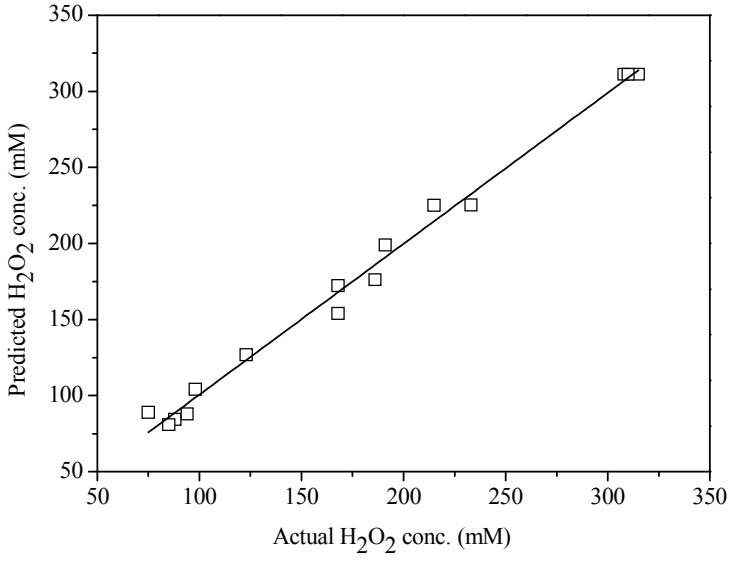


Fig. 6 Regression plots of actual data against predicted values from the response surface models describing $H_2O_2$ concentration.

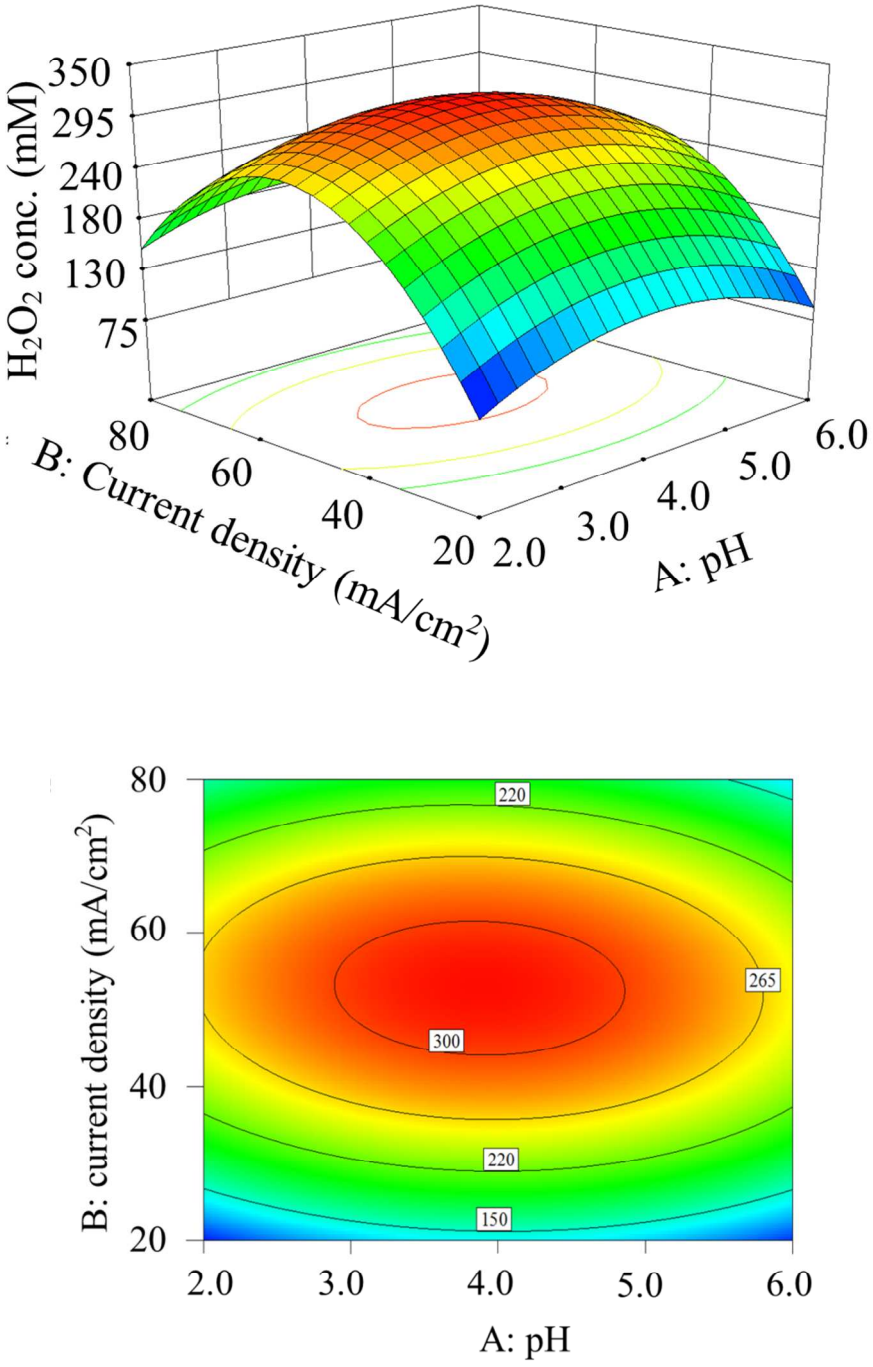


Fig. 7 Response surface plot and contour plot of $H_2O_2$ concentration as the function of initial pH and current density. Reaction conditions: air flow rate 50 mL/min, electrolytic time 60 min.

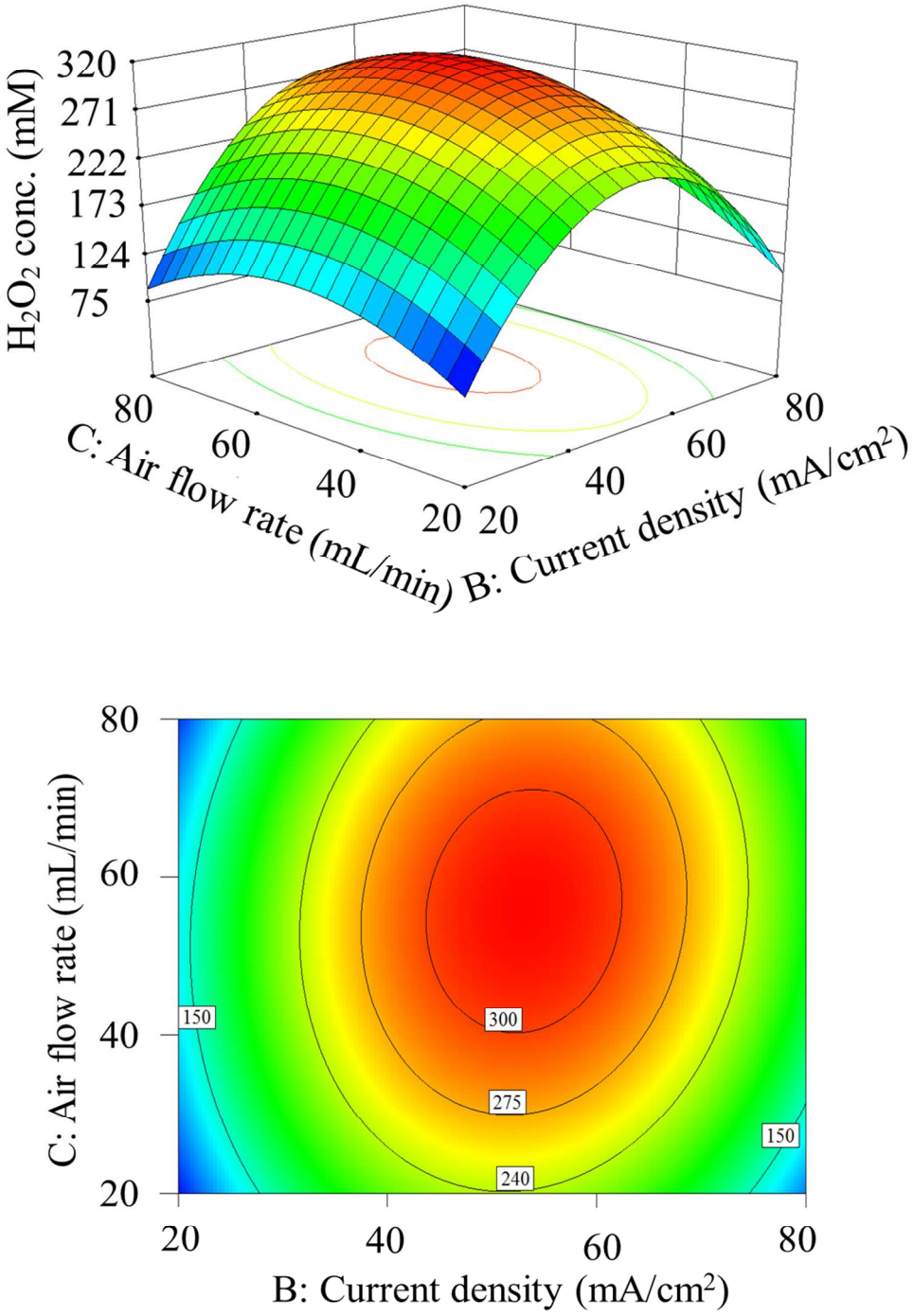


Fig. 8 Response surface plot and contour plot of $H_2O_2$ concentration as the function of current density and gas flow rate. Constant conditions: initial pH 4.0 , electrolytic time 60 min.

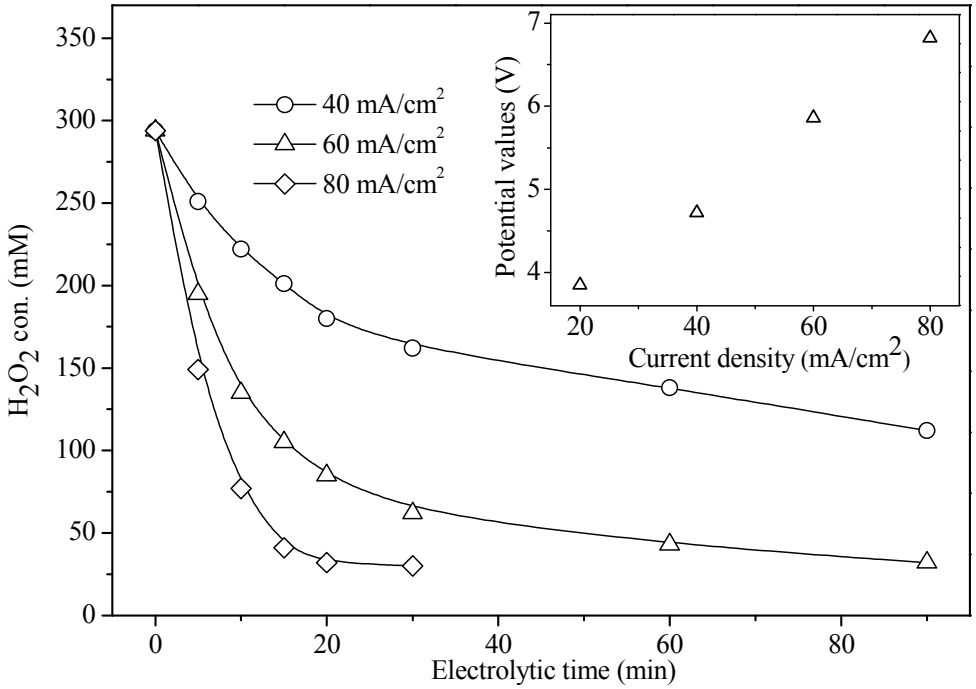


Fig. 9 $H_2O_2$ decomposition as the function of electrolytic time

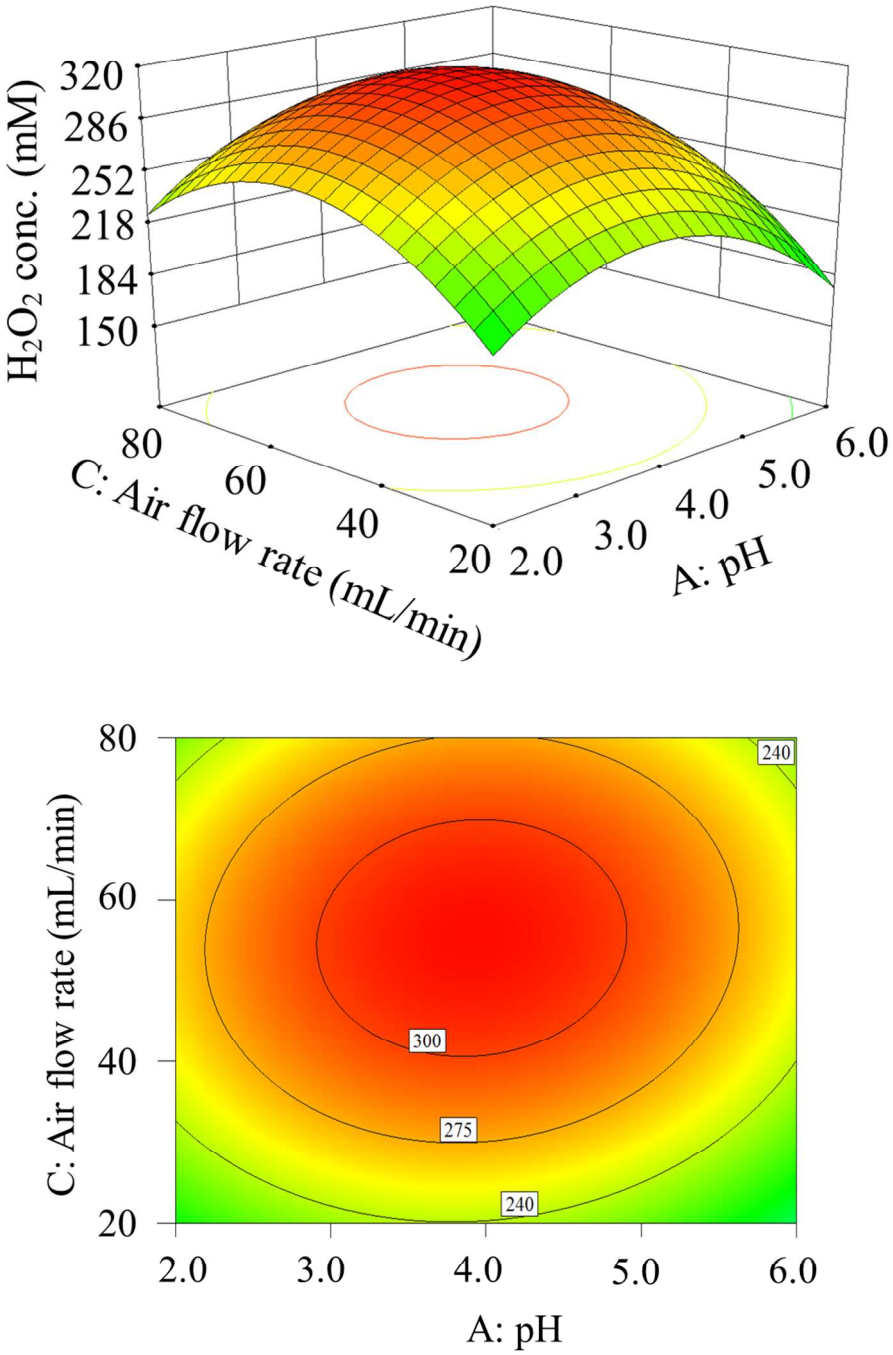


Fig. 10 Response surface plot and contour plot of $H_2O_2$ concentration as the function of initial pH and air flow rate. Constant conditions: current density 50 mA/cm$^2$, electrolytic time 60 min.

Table 1 Factor levels for the experiments.

| Process variables | Code | Real values of coded levels | | |
|---|---|---|---|---|
| | | -1 | 0 | +1 |
| Initial pH | A | 2 | 4 | 6 |
| Current density ($mA/cm^2$) | B | 20 | 50 | 80 |
| Gas flow rate (ml/min) | C | 20 | 50 | 80 |

Table 2 Experimental design matrix by BBD design and response on $H_2O_2$ concentration.

| Run | pH | Current density ($mA/cm^2$) | Gas flow rate (mL/min) | $H_2O_2$ conc. (mM) |
|---|---|---|---|---|
| 1 | 6.0 | 20 | 50 | 75.51 |
| 2 | 2.0 | 50 | 20 | 191.26 |
| 3 | 4.0 | 50 | 50 | 308.41 |
| 4 | 6.0 | 50 | 20 | 186.51 |
| 5 | 6.0 | 50 | 80 | 233.25 |
| 6 | 4.0 | 80 | 80 | 167.92 |
| 7 | 6.0 | 80 | 50 | 123.25 |
| 8 | 4.0 | 50 | 50 | 310.62 |
| 9 | 4.0 | 20 | 20 | 85.17 |
| 10 | 2.0 | 80 | 50 | 168.81 |
| 11 | 4.0 | 80 | 20 | 98.27 |
| 12 | 4.0 | 20 | 80 | 94.35 |
| 13 | 2.0 | 20 | 50 | 88.42 |
| 14 | 4.0 | 50 | 50 | 315.17 |
| 15 | 2.0 | 50 | 80 | 215.21 |

Table 3 Performance comparison with literatures.

| Electrode structure | Configuration | Time | $H_2O_2$ conc. | Ref. |
|---|---|---|---|---|
| Sheet | Stainless steel mesh, Acetylene black-PTFE film | 450 min | 1130 mg/L | 14 |
| Sheet | Oxygen-fed graphite/PTFE, 2-ethylanthraquinone | 2 h | 414 mg/L | 13 |
| GDE | Silver-plated nickel web, XC-72 Carbon layers, Acetylene Black layers | 6000 s | 0.12 M | 11 |
| Dual GDE | Carbon fiber, Diffusion layer, Catalyst layer | 180 min | 1928 mg/L | 9 |
| GDE | Carbon black layer, Tert-butyl-anthraquinone | 90 min | 301 mg/L | 10 |
| GDE | Nickel mesh, Carbon-PTFE layer | 60 min | 12 mM | 12 |
| GDE | Titanium meshes, Conductive catalytic layer | 2 h | 315.67 mM | Present work |

Table 4 ANOVA test for the quadratic models.

| Source of variations | Sum of squares | DF | F-value | P-value |
|---|---|---|---|---|
| Model | 90546.72 | 9 | 450.02 | < 0.0001 |
| Residual | 89.42 | 4 | | |
| Lack of fit | 65.66 | 2 | 2.76 | 0.2657 |
| Pure error | 23.76 | 2 | | |
| Total | 90636.15 | 13 | | |

Table 5 statistical parameters obtained from the analysis of variance for the regression models.

| Response | $R^2$ | Adj. $R^2$ | CV | S.D. | A. P. | PRESS |
|---|---|---|---|---|---|---|
| $H_2O_2$ conc. | 0.9990 | 0.9968 | 2.56 | 4.73 | 56.747 | N/A |

A.P.: adequate precision; S.D.: standard deviation; CV: coefficient of variance; PRESS: predicted residual error sum of squares.

Table 6 Optimum conditions of the process variables for maximum $H_2O_2$ concentration.

| Initial pH | Current density ($mA/cm^2$) | Gas flow rate (mL/min) | $H_2O_2$ concentration (mM) | |
|---|---|---|---|---|
| | | | Actual | Predicted |
| 4.0 | 52 | 55 | 309.85 | 313.72 |